



## Pharmaceutical Nanotechnology

# Encapsulation of paclitaxel into lauric acid-*O*-carboxymethyl chitosan-transferrin micelles for hydrophobic drug delivery and site-specific targeted delivery



Joung-Pyo Nam<sup>1</sup>, Seong-Cheol Park<sup>1</sup>, Tae-Hun Kim, Jae-Yeang Jang, Changyong Choi, Mi-Kyeong Jang\*\*, Jae-Woon Nah\*

Department of Polymer Science and Engineering, Suncheon National University, 255 Jungang-ro, Suncheon, Jeollanam-do, Republic of Korea

## ARTICLE INFO

## Article history:

Received 24 June 2013

Received in revised form 16 August 2013

Accepted 11 September 2013

Available online 26 September 2013

## Keywords:

Transferrin

*O*-carboxymethyl chitosan

Micelle

Paclitaxel

PEG

## ABSTRACT

Transferrin/PEG/*O*-carboxymethyl chitosan/fatty acid/paclitaxel (TPOCFP) micelles were tested for suitability as a drug carrier characterized by low cytotoxicity, sustained release, high cellular uptake, and site-specific targeted delivery of hydrophobic drugs. Characterization, drug content, encapsulation efficiency, and in vitro drug release were investigated. When the feeding amount of paclitaxel (PTX) was increased, the drug content increased, but loading efficiency decreased. TPOCFP micelles had a spherical shape, with a particle size of approximately 140–649 nm. In vitro cell cytotoxicity and hemolysis assays were conducted to confirm the safety of the micelles. Anticancer activity and confocal laser scanning microscopy (CLSM) were used to confirm the targeting efficiency of target ligand-modified TPOCFP micelles. Anticancer activity and CLSM results clearly demonstrated that transferrin-modified TPOCFP micelles were quickly taken up by the cell. The endocytic pathway of TPOCFP micelles was analyzed by flow cytometry, revealing transfection via receptor-mediated endocytosis. These results suggest that PTX-encapsulated TPOCFP micelles may be used as an effective cancer-targeting drug delivery system for chemotherapy.

© 2013 Elsevier B.V. All rights reserved.

## 1. Introduction

Chemotherapy is a commonly used strategy for cancer treatment. Nevertheless, the use of a chemotherapeutic agent can be limited by poor solubility, low stability, short half-life, poor physiochemical properties, and high toxicity in normal cells and tissues (Hong et al., 2010). A drug delivery system (DDS) represents a method for optimizing the efficient administration of a pharmaceutical compound to achieve a therapeutic effect, particularly in cancer therapy (Wang and Recum, 2011). In the design of a drug delivery system, drug absorption, drug distribution, and drug release profile should be considered, while aiming to optimize therapeutic effects, patient convenience, and safety. Recently research on drug delivery system has focused on determining the

optimal speed of drug release and improving targeting ability so as to enhance drug delivery capability (Liu et al., 2008). Therefore, the development of drug delivery systems (DDS) has taken various forms, including micelles (Yokoyama, 1992), liposomes (Senior, 1987), monoclonal antibodies (Huennekens, 1994), macromolecules (Vincent Lee et al., 1995), and targeting ligands (Perales et al., 1994). Each of these methodological approaches has aimed to prolong and maintain efficient plasma concentrations of the materials and maximize site-specific targeting.

Targeting to specific cells or tissues is a characteristic of a DDS, and necessary for preventing nonspecific delivery into healthy cells or tissues and minimizing potential side effects identified from in vitro or in vivo analyses. Previously reports have described surface modifications of carrier materials that improve their targeting ability (Perales et al., 1994). In addition, Sahu et al. (2011a, 2010, 2012) reported that targeting ligand (as a folic acid) modified amphiphilic biodegradable polymers significantly enhances the cellular uptake by targeting ligand and effectively delivered anticancer drug as a doxorubicin.

Transferrin (TF), a naturally existing protein, has received significant attention in the development of drug targeting systems. TF has biodegradable, nontoxic, and non-immunogenic properties, and can achieve site-specific targeting due to the high levels of TF receptors (TfR) present on the cell surface (Qian et al., 2002). The

\* Corresponding author at: Department of Polymer Science and Engineering, Suncheon National University, Suncheon, Republic of Korea. Tel.: +82 61 750 3566; fax: +82 61 750 5423.

\*\* Corresponding author at: Department of Polymer Science and Engineering, Suncheon National University, Suncheon, Republic of Korea. Tel.: +82 61 750 3567; fax: +82 61 750 5423.

E-mail addresses: [jmk8856@suncheon.ac.kr](mailto:jmk8856@suncheon.ac.kr) (M.-K. Jang), [jwnah@suncheon.ac.kr](mailto:jwnah@suncheon.ac.kr) (J.-W. Nah).

<sup>1</sup> These authors contributed equally to this study.

TfR facilitates iron uptake into vertebrate cells through a cycle of endo- and exocytosis of TF (Richardson and Ponka, 1997). Elevated expression of TfRs in malignant cells has been attributed to their requirement for high concentrations of iron for growth (Huebers and Finch, 1987). TF/TfR-mediated cellular events have also been exploited in carrier systems that deliver therapeutic drugs and genes into malignant cells that overexpress TfR (Li and Qian, 2002). In this study, the surface of the micelle was modified by attaching TF, to facilitate receptor-mediated endocytosis via the TfR.

PTX is an anticancer drug that stabilizes microtubules, therefore interfering with the normal breakdown of microtubules during cell division. PTX has demonstrated significant antitumor activity in clinical trials when tested against a broad range of solid tumors, especially non-small lung cancer, metastatic breast cancer, ovarian cancer and advanced forms of Kaposi's sarcoma (Kim et al., 2001; Singla et al., 2002). However, PTX has serious side effects including allergic reactions, neurotoxicity, hypersensitivity, nephrotoxicity, and labored breathing in patients, caused by the Cremophor EL-based formulation that is used counter the poor solubility of PTX (Yao et al., 2011). Therefore, many researchers have studied alternative formulations that include nanoparticles, liposomes, dendrimers, micelles, polymeric drugs, and microspheres as replacements for Cremophor EL.

O-carboxymethyl chitosan (OCMCh) is a carboxymethylated derivative of chitosan that possesses a CH<sub>2</sub>COOH modification at the C6 position of chitosan. OCMCh has good biocompatibility, bioactivity, antibacterial activity, solubility in aqueous solutions, and stability properties that have been reported previously (Chen and Park, 2003; Liu et al., 2001; Chen et al., 2005). Therefore, OCMCh is an extensively used in a wide range of biomedical field as a drug carrier (Sahu et al., 2010, 2011b, 2012). However, OCMCh used in our study was prepared using LMWSC which has free-amine group unmodified with any functional group (Nah and Jang, 2002). It is easy to modify with functional group because LMWSC with free amine group has high reactivity. OCMCh increases the flexibility of chitosan molecular chains in water (Yin et al., 2004), and has multifunctional groups such as NH<sub>2</sub> and COOH the latter created by carboxymethylation. The multifunctional groups within of OCMCh can be used for various modifications including linkages to proteins, drugs, genes, targeting ligands, antibodies, and pH-sensitive bond. Therefore, OCMCh has applications in the biomedical and pharmaceutical fields. In our previous reports, we prepared low molecular weight OCMCh characterized its various functions using NMR (Nam et al., 2008).

In the present study, the hydrophobic moiety fatty acid (FA, lauric acid) was coupled to the NH<sub>2</sub> position of OCMCh using NHS and EDC, creating the hydrophobic drug delivery carrier OCMCh-FA (OCF). PTX was then encapsulated into the OCF micelle via hydrophobic interactions. In addition, PEGylated transferrin (TP) was covalently attached to OCF for specific-site target delivery and receptor-mediated endocytosis. The drug content, encapsulating efficiency, and in vitro drug release of PTX-encapsulated OCF micelles (OCFP) were investigated, and the particle size and morphology of TP-conjugated OCFP (TPOCFP) were determined. The targeting ability, hemolysis, and cytotoxicity of TPOCFP were investigated. The anticancer activities and endocytic pathway of TPOCFP micelles were evaluated using the MTT assay and the FACS assay.

## 2. Materials and methods

### 2.1. Materials

O-carboxymethyl chitosan (OCMCh, Mw = 12,000 Da, degree of deacetylation greater than 95.0%) was prepared as previously described. 1-Ethyl-3-(3-dimethylaminopropyl)

carbodiimide (EDC) and N-hydroxysuccinimide (NHS) were purchased from Sigma-Aldrich, Korea. Paclitaxel (PTX) was purchased from Samyang, Korea. TfR-targeting peptides (TF, THRPPMWSPVWPGGG-COOH) were synthesized using Fmoc solid-phase methods on a Liberty microwave peptide synthesizer (CEM Co., Matthews, NC). NH<sub>2</sub>-poly(ethylene glycol)-COOH (NH<sub>2</sub>-PEG-COOH, Mw = 3400) was purchased from SunBio, Korea. Red blood cells (RBCs) were obtained from an inbred rat (Orientbio Inc., Korea). LysoTracker and Hoechst 33258 were purchased from Invitrogen. NHS-rhodamine was purchased from Thermo Scientific. Dulbecco's modified eagle medium (DMEM), Roswell park memorial institute (RPMI)-1640, and fetal bovine serum were obtained from Gibco (BRL, MD, USA). 3-(4,5-Dimethyl-2-thiazolyl)-2,5-diphenyl-2H-tetrazolium bromide (MTT) and trypsin were also purchased from Sigma-Aldrich (St. Louis, MO). All solvents used in this investigation were of HPLC grade. All other chemicals and solvents were analytical or reagent grade and used without further purifications.

### 2.2. Methods

#### 2.2.1. Cells and cell culture conditions

Human colon cancer cell lines (LoVo, DLD-1, CoLo 255, and HCT 119), human prostate cancer cells (PC3), human breast cancer cells (SK-Br3), and human embryonic kidney cells (HEK 293) were maintained in RPMI-1640 or DMEM supplemented with 10% FBS at 37 °C in a humidified atmosphere containing 5% CO<sub>2</sub>. Cells grown as a monolayer were harvested by trypsinization (trypsin-EDTA). The using cell lines, including LoVo, DLD-1, CoLo 255, HCT 119, PC3, SK-Br3, and HEK 293, were purchased from KCLB® (Seoul, Republic of Korea).

#### 2.2.2. Synthesis of O-carboxymethyl chitosan (OCMCh)

OCMCh was synthesized according to a previously reported method (Nam et al., 2008). In brief, 2 g of the low molecular weight water-soluble chitosan (LMWSC) was immersed in 25 mL of 50% (w/v) NaOH solution and alkalinized for 24 h. The alkalinized LMWSC was filtered and then transferred into a flask. To this flask, 5 g of monochloroacetic acid dissolved in 25 mL of isopropanol was added in a dropwise manner over 20 min. This flask was allowed to react further for 8 h at room temperature. The reactants were subsequently filtered to remove the solvent. The filtrates were dissolved in 100 mL of water and the pH was adjusted to 5.0 by using 1 N-HCl solution. An excess amount of 80% ethanol was added to precipitate the product. The precipitates were harvested by filtration and rinsed 3 times with 80% ethanol followed by vacuum-drying at room temperature.

#### 2.2.3. Fatty acid-modified OCMCh (OCF)

OCMCh (100 mg) was dissolved in 10 mL of deionized water. FA, the hydrophobic moiety of lauric acid C12 (9.1 mg), was dissolved in 3 mL of ethanol. EDC (26.1 mg) was added dropwise into the FA/ethanol solution while stirring at room temperature. After 10 min, NHS (15.6 mg) was added dropwise into the EDC/FA solution while stirring at room temperature for 1 h. The NHS-activated FA solution was slowly added dropwise into the OCMCh solution while stirring at room temperature for 24 h. After 24 h, the FA-modified OCMCh (OCF) was precipitated with 80% ethanol. The precipitated material was dried at room temperature and then dissolved in 10 mL of distilled. The resulting solution was dialyzed against distilled water for 2 d by using a 3500 g/mol molecular weight cut-off (MWCO) dialysis membrane to remove the unreacted materials, and then lyophilized.

### 2.2.4. Preparation of PTX-encapsulated micelles

PTX-encapsulated OCF micelles (OCFP) were prepared by hydrophobic interaction using sonication (Wang et al., 2007). OCF was dispersed in water while shaking gently at room temperature for 30 min. PTX (5 and 10 mg) was dissolved in 1 mL of acetone, and then added to the dispersed solution of OCF while shaking gently at room temperature for 30 min. This step was followed by sonication for 30 min in an ice bath using a probe-type sonifier (Automatic Ultrasonic Processor VCX-400/600, USA) at 30 W, with a pulse function of 2.0 s on and 3.0 s off. The final solutions were filtered through a 0.8- $\mu$ m filter (Millipore) to remove insoluble product and dust. Then, powders of PTX-encapsulated OCF micelles (designated OCFP 5 and OCFP 10, for 5 and 10 mg of encapsulated PTX, respectively) were obtained by lyophilization.

### 2.2.5. Synthesis of transferrin-polyethylene glycol (TP)

The target ligand for TfR, TF (48 mg), was dissolved in 5 mL of distilled water. EDC (11.7 mg) was added dropwise into the TF solution while stirring at room temperature. After 10 min, NHS (7.0 mg) was added dropwise into the EDC-TF solution while stirring at room temperature for 1 h. The NH<sub>2</sub>-PEG-COOH form of PEG (100 mg) was dissolved in 20 mM HEPES buffer. The NHS-activated TF solution was slowly added dropwise to the PEG solution while gently stirring at room temperature for 2 h. After 2 h, TF-conjugated PEG (TP-COOH) solution was dialyzed against distilled water for 2 d by using a 3000 g/mol MWCO dialysis membrane to remove unreacted transferrin, EDC, and NHS. The final product was obtained through lyophilization.

### 2.2.6. TP-modified OCFP micelles

TP-modified OCFP micelles (TPOCFP) were prepared by ion-complexation between the COOH position of TP and NH<sub>2</sub> position of OCFP. The TP solution was added dropwise into the OCFP solution while stirring at room temperature for 30 min. After 30 min, TPOCFP micelles were used to confirm cellular uptake, investigate cytotoxicity, in vitro drug release, and anticancer activity, and utility in a flow cytometry assay. The final amount of TP that was modified was 1%.

### 2.2.7. Characterization of OCFP and TPOCFP micelles

The prepared OCFP was characterized by <sup>1</sup>H NMR and Fourier transform infrared spectroscopy (FT-IR). The <sup>1</sup>H NMR spectra of products were measured in deuterium oxide (D<sub>2</sub>O) and dimethyl sulfoxide (DMSO) using a 400 MHz NMR spectrometer (AVANCE 400FT-NMR 400 MHz, Bruker). OCMCh, OCF, OCFP 5, and OCFP 10 (5 mg of each) were dissolved in 0.5 mL of D<sub>2</sub>O. In addition, OCFP 5 and OCFP 10 (5 mg of each) were dissolved in 0.5 mL of the cosolvent D<sub>2</sub>O/DMSO (2:8) to decomplexed nanoparticles, and the products were assessed using an NMR spectrometer.

OCMCh, OCF, OCFP 5, OCFP 10, as well as the physical mixture of OCF and PTX (1 mg each) were mixed with 100 mg of KBr (1:100, weight ratio). FT-IR spectra were obtained on an 8700 FT-IR spectrophotometer (Shimadzu, Japan) using the powder form of each micelle on KBr discs ranging from 400 to 4600 cm<sup>-1</sup>.

The average particle size and size distribution of OCFP and TPOCFP micelles were determined using an ELS-8000 electrophoretic LS spectrophotometer (NICOMP 380 ZLS zeta potential/particle sizer; Otsuka Electronics Inc., Japan) equipped with a He-Ne laser beam at a wavelength of 632.8 nm at 25 °C (scattering angle of 90°). A sample solution (1 mg/mL) was used for the particle measurement (HE. 013.016-ALU cell adapter) without filtering.

To observe the morphology of the micelles, 2  $\mu$ L of OCFP or TPOCFP micelles suspended in deionized water were placed on a carbon film coated on a copper grid and stained with 1% uranyl acetate for 30 s. The grid was allowed to dry for 10 min and then

examined with a JEOL JEM-2000 FX-II transmission electron microscope (TEM).

The PTX concentrations of OCFP and TPOCFP micelles were determined using HPLC analysis (Liang et al., 2012). The HPLC system consisted of a mobile phase delivery pump (LC-20AD HPLC pump, Shimadzu, Japan) and a UV detector (SPD-20A, UV/vis detector, Shimadzu, Japan). For separation of components, a ZORBAX 300SB-C18 reverse-phase column (250 mm  $\times$  4.6 mm, 5  $\mu$ m, Agilent Technologies Inc., USA) was used. The mobile phase was composed of acetonitrile and water at a ratio of 40:60 (v/v). The flow rate and column temperature were set at 1.0 mL/min and 30 °C, respectively. The UV absorbance was determined at 227 nm with an injection volume of 20  $\mu$ L. The drug concentration of PTX was calculated from standard curves. The assay was linear over the tested concentration range. The drug contents (DC) and encapsulating efficiency (EE) were calculated as following:

$$\text{DC\%} = \frac{\text{Weight of the drug in micelles}}{\text{Weight of the feeding polymer and drug}} \times 100$$

$$\text{EE\%} = \frac{\text{Weight of the drug in micelles}}{\text{Weight of the feeding drug}} \times 100$$

### 2.2.8. Profile of PTX release from TPOCFP in vitro

The profile of PTX release from TPOCFP micelles was measured as follows. TPOCFP 5 and TPOCFP 10 (1 mg each) were dissolved in phosphate buffer (pH 5.2, 6.4, and 7.4) at each time point (0.5–48 h). The solution was added into the ultra-cellulose filter (Regenerated Cellulose 3000 MWCO, Microcon YM-10), and centrifuged at 12,000 rpm for 10 min and the amount PTX measured using HPLC.

### 2.2.9. In vitro cell cytotoxicity and anticancer activity

The cell cytotoxicity and anticancer activity of PTX-encapsulated OCFP 5 and OCFP 10 micelles, free drug (PTX in DMSO), and target ligand (TP)-modified TPOCFP 5 and TPOCFP 10 micelles were assessed using an MTT assay in against various cell lines (both normal cells and cancer cells). The experiment was carried out as follows: 50  $\mu$ L of cells in the growth phase were seeded into a 96-well micro plate at a density of 5  $\times$  10<sup>3</sup> cells/well. The DMEM and RPMI 1640 were supplemented with 10% fetal bovine serum (FBS) and 1% penicillin-streptomycin. Cells were incubated at 37 °C in a humidified atmosphere containing 5% CO<sub>2</sub>. When the cell confluence reached 75%, the cells were treated with select agents for 24 h at the equivalent drug concentrations of 0.002–0.125 mg/mL. After incubation, 10  $\mu$ L of MTT solution (5 mg/mL in PBS) was added to each well, and the plate was incubated for an additional 2 h at 37 °C. At the determined time, unreacted MTT was removed by aspiration. After removing the MTT-containing medium, the formazan crystals formed in live cells were dissolved with 100  $\mu$ L DMSO. Finally, the absorbance was measured at 570 nm (optical density) and 670 nm (for background subtraction). The relative cell viability (%) was calculated according to the following equation: OD value = (OD 560–OD 670)

$$\text{Relative cell viability (\%)} = \frac{(\text{OD sample} - \text{OD blank})}{(\text{OD control} - \text{OD blank})} \times 100$$

### 2.2.10. In vitro hemolysis test

The hemolysis test evaluates in vitro hemolytic activity of PTX-encapsulated TPOCFP 5 and TPOCFP 10 micelles following prolonged exposure with blood. The method for the hemolysis assay has been previously described by Burt et al. (1999). Inbred rat whole blood was used within 24 h after removing fibrinogen and washing 2 times in Dulbecco's phosphate buffered saline (D-PBS). After each washing, the supernatant was discarded and cells were pelleted by centrifugation at 2000 rpm for 5 min. The final pellet was

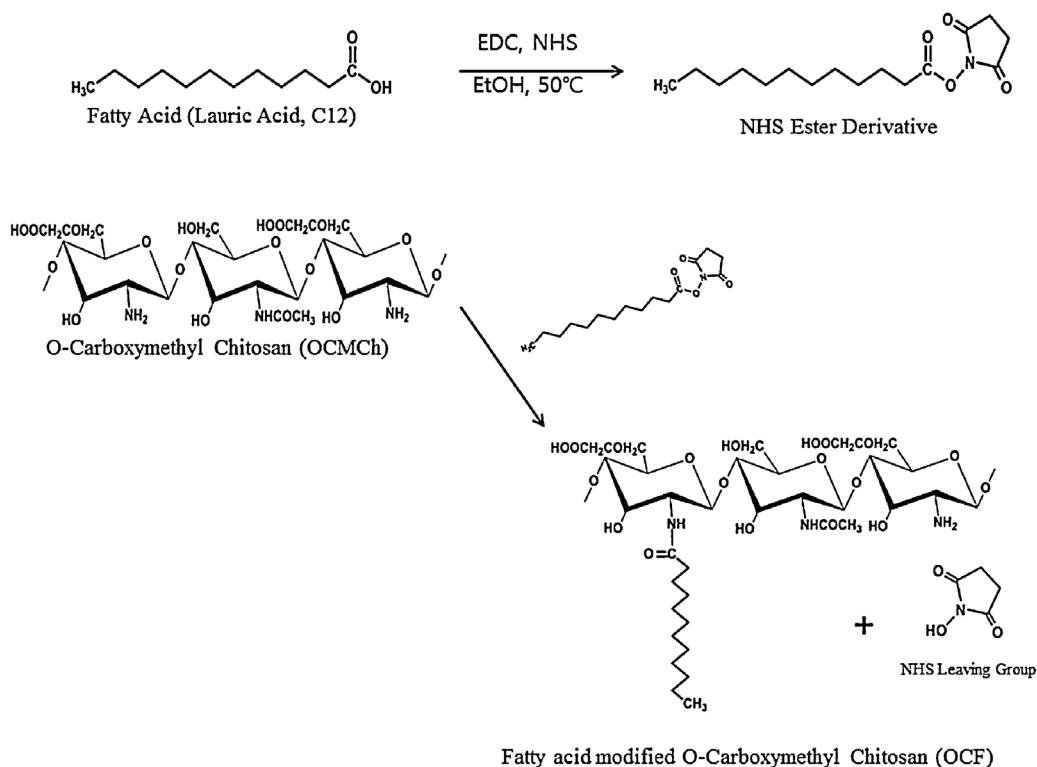


Fig. 1. Scheme of FA-coupled OCF with coupling agent for hydrophobic interaction with hydrophobic drug.

diluted with D-PBS to obtain an 8% suspension (v/v). For analysis, various concentrations of TPOCF5 and TPOCFP 10 micelles were dispersed in D-PBS and 100  $\mu$ l of the mixture was added to a microfuge tube together with 100  $\mu$ l of an 8% erythrocyte suspension. The final concentration of TPOCFP 5 and TPOCFP 10 micelles ranged from 0.625 to 1 mg/mL. Following this step, an incubation time of 4 h at 37 °C was tested. After this period of incubation, the samples were centrifuged at 2000 rpm for 2 min, and the supernatant was carefully collected taking care not to disturb the pellet. The absorbance of the supernatant was measured with D-PBS (negative control/NC) and 0.1% triton-X (positive control/PC) at 414 nm (VersaMax ELISA Microplate Reader; StakMax<sup>®</sup>, USA). The hemolytic levels were expressed as a percentage of hemolysis. The degree of hemolysis was calculated according to the following equation:

$$\text{Hemolysis (\%)} = \frac{(\text{OD}_{\text{sample}} - \text{OD}_{\text{NC}})}{(\text{OD}_{\text{PC}} - \text{OD}_{\text{NC}})} \times 100$$

#### 2.2.11. Analysis of micelle distribution using confocal laser-scanning microscopy

In order to analyze cellular distribution, OCFP and TPOCFP micelles were examined with confocal laser-scanning microscopy (CLSM). OCFP and TPOCFP were labeled with NHS-rhodamine (10  $\mu$ M) and endosomes were labeled with LysoTracker Green DND-189 (1  $\mu$ M). Subsequent to the addition of the complexes, the cells were incubated for 1 h and then washed with PBS (2  $\times$  1 mL). Cells were pre-incubated with Hoechat 33258 probes to detect intracellular localization of micelles. Localization of rhodamine-labeled micelles was then determined using an inverted LSM510 laser scanning microscope (Carl Zeiss, Gottingen, Germany). To detect rhodamine-labeled micelles, LysoTracker, and DAPI, the 405 nm lines of the diode laser and the light of 511 and 543 nm helium neon lasers were directed over a UV/488/543/633 beam splitter. Images were recorded digitally using a 512  $\times$  512 pixel format.

#### 2.2.12. Flow cytometry assay (FACS)

Flow cytometry (FACSCanto II, BD, USA) was used to analyze both cellular uptake and endocytic pathways of rhodamine-labeled OCFP and TPOCFP micelles. CoLo-255 cells were seeded in 6-well plates and incubated for 24 h. Following incubation, the cells were rinsed twice with fresh medium, and different cellular entry inhibitors such as chlorpromazine, indomethacin, sodium azide, and colchicin were added to each well. After incubation for 2 h, the inhibitors were removed OCFP or TPOCFP micelles were added, and cells were incubated at 37 °C for 4 h. At the end of the incubation period, the cells were washed with PBS and a stripping solution, trypsinized, and collected into 15 mL centrifuge tubes for FACS analysis.

#### 2.2.13. Statistical analysis

Statistically significant differences were determined using Student's *t*-test, or one-way analysis of variance (ANOVA), with *p* values of <0.05 indicating statistically significant differences.

### 3. Results

#### 3.1. Characterization of OCFP and TPOCFP micelles

The FA-modified OCMCh was synthesized by chemical reaction with coupling agent for hydrophobic drug incorporation (Fig. 1). The OCF formed self-assembled micelles by hydrophobic interaction with a core-shell structure (Fig. 2). In addition, TPOCFP micelles were prepared to confirm receptor-mediated endocytosis between TF and the TfR present at the surface of the cancer cell.

The characterization of OCFP and TPOCFP was conducted using <sup>1</sup>H NMR, FT-IR, dynamic light scattering (DLS) and TEMs. The <sup>1</sup>H NMR result for OCFP is shown in Fig. 3. The proton peaks of OCMCh from position C1 to C7 were classified between 2.8 and 5.0 ppm, and peak assignments were as follows (Fig. 3A): C1 position, 4.7 ppm; C2 position, 2.8 ppm; C3–C6 position, 3.2–3.6 ppm; C7 position,

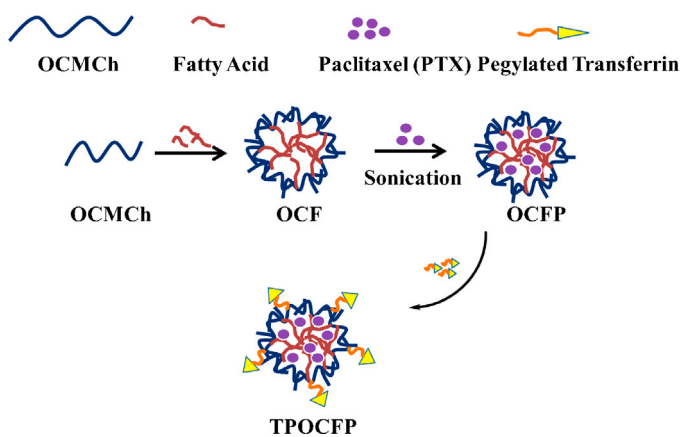


Fig. 2. Schematic illustration of PTX-encapsulated TPOCFP for hydrophobic drug delivery.

3.7 ppm; acetyl group position, 2.1 ppm. In Fig. 3B, the proton peaks of FA from position a to K were classified between 0.5 and 3.5 ppm, and peak assignments were as follows: a position, 1.3 ppm; b–e positions, 0.8 and 1.2 ppm; f, g, i, and j positions 2.1 and 2.3 ppm; k position, 3.3 ppm. In Fig. 3C, the proton peaks of OCMCh and FA were assigned. In addition, the proton peaks of position C7 OCMCh and the position of FA were shifted due to the FA modification of OCMCh. Fig. 3 indicates that FA was produced during the coupling reaction. Fig. 4 shows the proton peak of hydrophobic drug-encapsulated OCFP by  $^1\text{H}$  NMR. As in Fig. 4C, the proton peak of PTX, encapsulated in OCF by hydrophobic interactions, did not appear in the  $\text{D}_2\text{O}$  solvent. On the other hand, as indicated in Fig. 4D, the proton peak of PTX appeared in the  $\text{D}_2\text{O}/\text{DMSO}$  (2:8) solvent after decomplexation by sonication.

As shown in Fig. 5, OCMCh, OCF, OCFP 5, OCFP 10, and the physical mixture (OCF with PTX) have intrinsic absorption peaks from 450 to  $3500\text{ cm}^{-1}$ . The absorption peaks of C–H at  $1250\text{ cm}^{-1}$ , N–H at  $1510\text{ cm}^{-1}$ ,  $\text{NH}_2$  at  $1640\text{ cm}^{-1}$ , and C=O at  $1610\text{ cm}^{-1}$  were characteristic of OCMCh (Fig. 5A). In comparison with OCF, the absorption peaks of C=O at  $1640\text{ cm}^{-1}$  were increased due to the carboxyl group of FA coupled to the  $\text{NH}_2$  group of OCMCh (Fig. 5B).

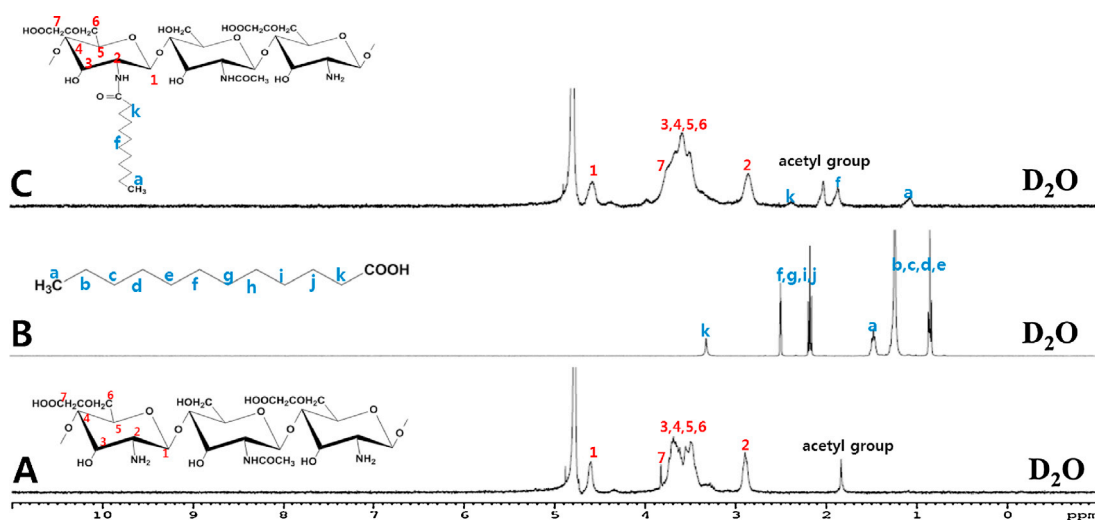


Fig. 3.  $^1\text{H}$  NMR spectra of OCMCh (A), FA (B), and OCF (C) in  $\text{D}_2\text{O}$  of NMR solvent.

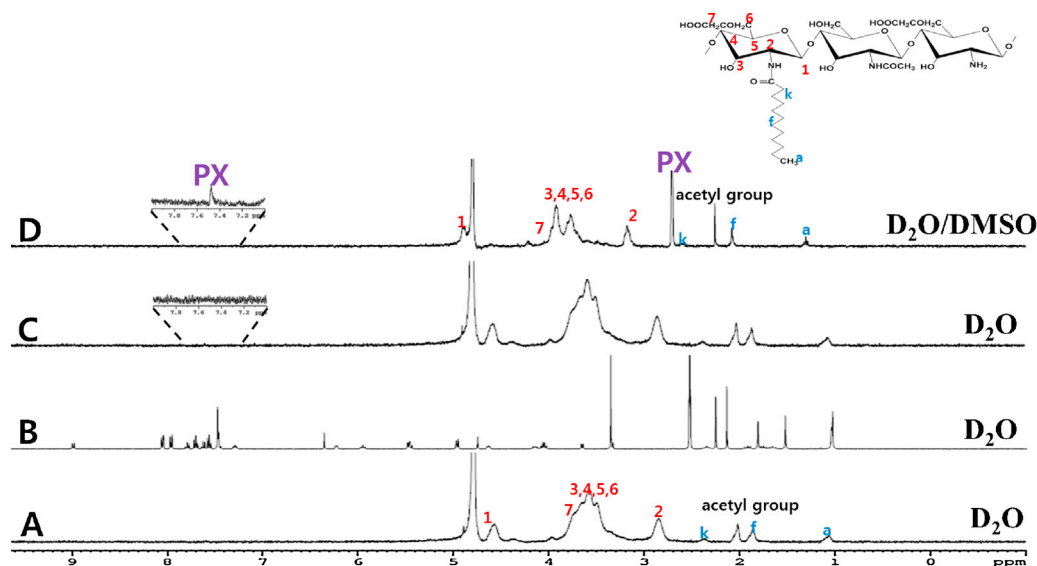
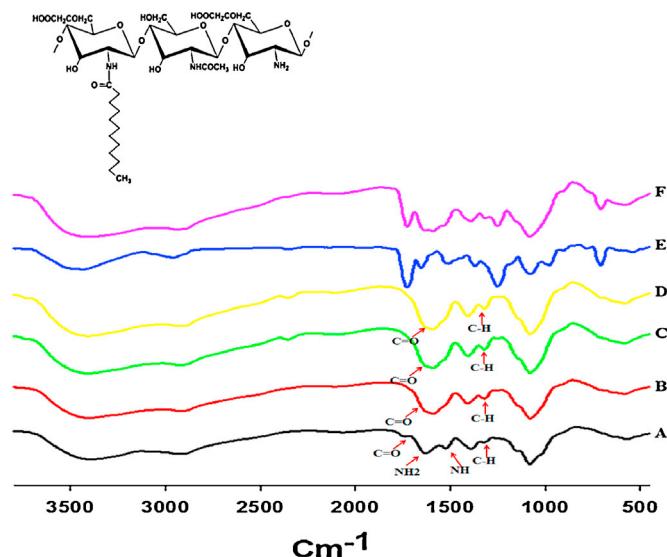


Fig. 4.  $^1\text{H}$  NMR spectra of OCF (A), PTX (B), OCFP (C) in  $\text{D}_2\text{O}$ , and OCFP (D) in  $\text{D}_2\text{O}/\text{DMSO}$  cosolvent (2:8) for decomplexation of OCFP micelles.



**Fig. 5.** FT-IR spectra of OCMCh (A), OCF (B), OCFP 5 (C), OCFP 10 (D), PTX (E), and OCF-PTX (physical mixture) (F).

The profiles of PTX-encapsulated OCFP 5 and 10 were similar to OCF, while the physical mixtures possessed all of the absorption peaks of OCF and PTX. These  $^1\text{H}$  NMR and FT-IR results demonstrated that PTX was successfully encapsulated into the OCF complex by hydrophobic interactions.

The particle size and morphology of OCFP and TPOCFP micelles were measured by DLS and TEM (Fig. 6). OCF, OCFP 5, and TPOCFP 5 had a uni-modal particle size distribution, while OCFP 10 and TPOCFP 10 had a di-modal particle size distribution. Table 1 shows that when the feeding amount of PTX and modified TFPEG was increased, particle size was increased due to hydrophobic drug being inserted into the core of OCF micelles, and OCFP being coated by TFPEG. The particle size of OCFP and TPOCFP micelles ranged from around 140 to 649 nm. Both OCFP and TPOCFP micelles have spherical shapes and smooth surfaces (Fig. 6). In addition, the observed particle size has similar particle size as indicated by the DLS results. The physicochemical characterization and drug incorporating parameters of TPOCFP 5 and 10 micelles are summarized in Table 2. When the feeding amount of PTX was increased, the drug content was increased, while the incorporating efficiency decreased. In addition, the yields were >85%.

### 3.2. *In vitro* drug release profile of TPOCFP micelles

In order to describe the release profile of PTX, the total amount of PTX released from TPOCFP in media as a function of pH was determined using HPLC. As shown in Fig. 7, PTX was slowly released from TPOCFP micelles according to the pH of the media (pH 5.2, 6.4, and 7.4). The accumulated release rate was less than 50% within 48 h. The release of TPOCFP micelles at pH 5.2 was faster than that of TPOCFP micelles at pH 6.4 or pH 7.4. In addition, the release of TPOCFP 10 was much slower than that of TPOCFP 5. However, this difference was not statistically significant. Interestingly, the burst-like release of TPOCFP 5 and TPOCFP 10 micelles at pH 5.2, 6.0, and 7.4 was not obvious. This phenomenon indicates that PTX was effectively encapsulated into the OCF.

### 3.3. *In vitro* cytotoxicity and hemolytic potential

In order to investigate the cytotoxicity of OCFP, TPOCFP, and free PTX, we have performed a cytotoxicity study using HEK 293 cells in an *in vitro* MTT assay. Following an incubation period of

48 h, we observed that when the encapsulated drug concentration of OCFP and TPOCFP was increased from 0.002 to 0.125 mg/mL, cell viability did not decrease to >80%, while free PTX decreased the cell viability (Fig. 8A). This result clearly demonstrated that the OCF carrier system decreased the cytotoxicity of PTX.

In order to determine whether TPOCFP micelles are safe for intravenous administration, the hemolytic potential of TPOCFP micelles was evaluated using a modified method of Burt et al. (1999). As shown in Fig. 8B, the drug concentrations tested in the assay ranged from 0.625 to 1 mg/mL. Hemolysis resulting from exposure to TPOCFP 5 or TPOCFP 10 was less than 5% at all drug concentrations, a rate suggesting very low hemolytic activity. The instability of carrier in the blood is considered to be one of the serious limitations in the therapeutic use of cationic polymers (Yang et al., 2012; Kainthan et al., 2006). However, OCMCh possesses a negative charge due to the carboxyl group. In addition, the  $\text{NH}_2$  group of OCMCh was modified by fatty acid and target ligand. Therefore, the TPOCFP carrier encapsulating PTX using OCMCh has a low rate of hemolysis due to its reduced positive charge.

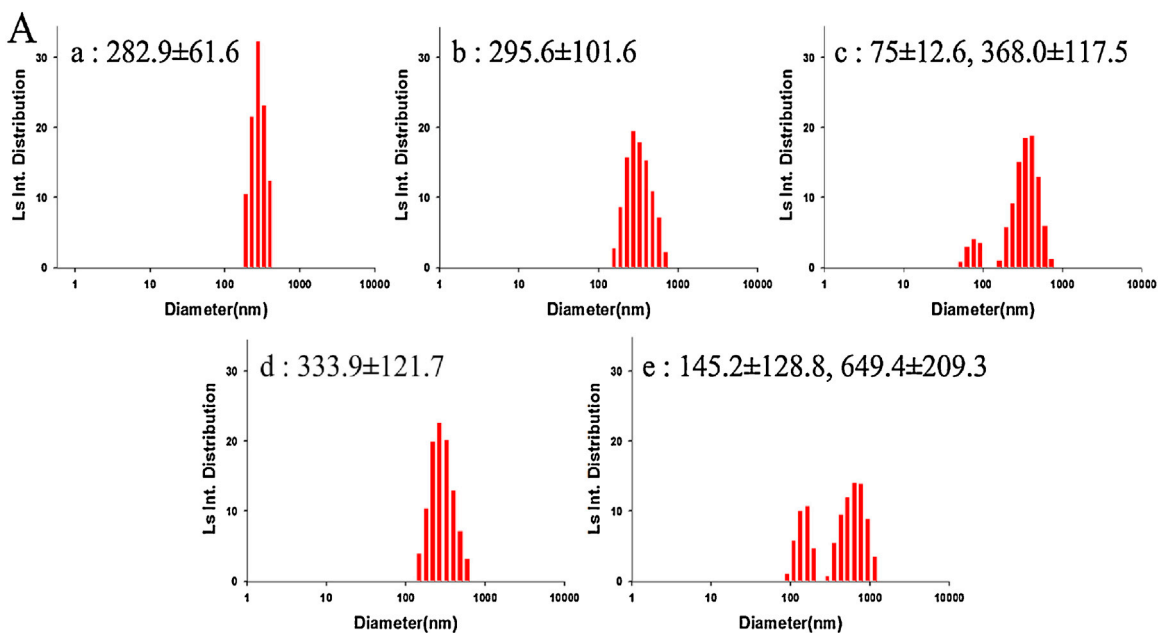
### 3.4. *In vitro* anticancer activity of OCFP and TPOCFP in various cancer lines

The MTT assay was employed to measure anticancer activity of OCF-PTX and TPOCF-PTX. The various cancer cells, including colon cancer, prostate cancer, and breast cancer cells, were treated with various formulations of OCFP and TPOCFP micelles at concentrations ranging from 0.002 to 0.125 mg/mL. The anticancer activity of OCFP and TPOCFP micelles are shown in Fig. 9. Except for the HCT 119 cells (Fig. 9C), the  $\text{IC}_{50}$  was 0.625 mg/mL of drug in all cancer cells. In the HCT 119 cells, the  $\text{IC}_{50}$  was 0.125 mg/mL. The anticancer activity of OCFP and TPOCFP micelles in LoVo, DLD-1, and PC3 cells was <20% at 0.125 mg/mL. However, other cells (CoLo 255, HCT 119, and SK-Br3 cells) showed more than 20% viability. In addition, when the amount of PTX incorporated into OCFP and TPOCFP micelles at 5–10 mg was increased, cell viability was decreased.

In comparison, cell viability of the OCFP was greater than TPOCFP. This result demonstrated that TPOCFP was effectively taken up into the cell by receptor-mediated endocytosis facilitated by the TF ligand of TPOCFP and the TfR present on the surface of the cancer cell.

### 3.5. Analysis of cellular uptake of OCFP and TPOCFP by CLSM

The confocal laser scanning microscopy (CLSM) study permitted the evaluation of the efficiency of intracellular uptake of TPOCFP as a function of target ligand in PC3 cells. In this study, FACS was conducted on using PC3 cells line to compare the effect of internalization by target ligand. As in Fig. 10, cellular uptakes of OCFP and TPOCFP were differently shown according to amount of PTX and treated amount of OCFP and TPOCFP into the cells. When the amount of encapsulated PTX and the feeding amount were increased, the fluorescence intensity of rhodamine and LysoTracker were increased. The TF-modified TPOCFP micelles were located in the nuclei of cells. However, the TF-unmodified OCFP micelles were observed to have a perinuclear location. These results clearly demonstrated the effect of target ligand, in that the TPOCFP micelles modified with target ligand had faster uptake into the nuclei of cells compared to the OCFP nanoparticles that were unmodified by target ligand. This phenomenon is hypothesized to reflect the effect of targeting mediated by binding of the TF-coupled TPOCFP to TfR present on the surface of cancer cells. Fig. 10 clearly shows this phenomenon in a merged image of OCFP 10 (100  $\mu\text{g}/\mu\text{L}$ ) and TPOCFP 10 (100  $\mu\text{g}/\mu\text{L}$ ).



**B**

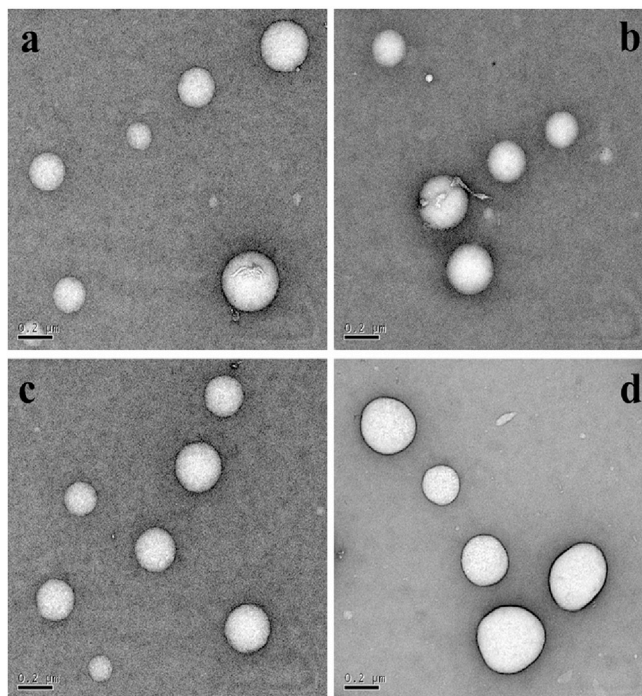


**Fig. 6.** (A) Particle size distribution of OCF (a), OCFP 5 (b), OCFP 10 (c), TPOCFP 5 (d), and TPOCFP 10 (e) by using DLS. (B) Morphological observation of OCFP 5 (a), OCFP 10 (b), TPOCFP 5 (c), and TPOCFP 10 (d) by using TEM.

**Table 1**  
Particle size of various micelles by DLS analysis.

Sample	Amount of polymer (mg)	Amount of drug (mg)	Particle size (nm)		
			Ls Int. (IS)	Wt conv. (wt)	No conv. (no)
OCF	–	–	$282.9 \pm 61.6$	$246.2 \pm 52.7$	$220.4 \pm 39.9$
OCFP 5	80	5	$295.6 \pm 101.6$	$219.6 \pm 66.7$	$181.3 \pm 42.1$
OCFP 10	80	10	$75 \pm 12.6, 368.0 \pm 117.5$	$68.6 \pm 12.3, 270.0 \pm 87.7$	$62.8 \pm 10.6, 214.7 \pm 54.6$
TPOCFP 5	80	5	$333.9 \pm 121.7$	$239.2 \pm 76.4$	$196.0 \pm 45.8$
TPOCFP 10	80	10	$145.2 \pm 128.8, 649.4 \pm 209.3$	$128.4 \pm 26.4, 477.5 \pm 151.9$	$114.8 \pm 21.7, 388.5 \pm 92.6$

**Table 2**  
Characterization of PTX-encapsulated TPOCFP micelles.

Sample	Amount of polymer (mg)	Amount of drug (mg)	Particle size (nm)	Drug content (%)	Encapsulation efficiency (%)	Yield (%)
TPOCFP 5	80	5	333.9 ± 121.7	2.1	32	90.4
TPOCFP 10	80	10	145.2 ± 128.8	2.9	22.6	85.3
			368.0 ± 117.5			

**3.6. FACS analysis of the mechanism of cellular entry by OCFP and TPOCFP**

TF, used as a targeting ligand, has the potential to bind to TfR present on the surface of cancer cells. Therefore, the cellular uptake of rhodamine-labeled TPOCFP micelles was significantly greater than rhodamine-labeled OCFP micelles (which did not possess TP) due to the targeting potential of ligand-receptor binding (Fig. 11A). However, cellular uptake was reduced by chlorpromazine (Fig. 11B). This result clearly showed that TPOCFP micelles were taken up by receptor-mediated endocytosis. Colchicine, sodium azide, and indomethacin did not reduce uptake TPOCFP micelles.

**4. Discussion**

The polymeric micelle has the potential for encapsulating materials within its core. The inner core of these micelles is typically hydrophobic, enabling successful encapsulation of hydrophobic drugs, while its hydrophilic shells make the encapsulated material soluble (Cho et al., 2008). Polymeric micelles include synthetic natural polymers (such as peptide, chitosan, and hyaluronic acid), synthetic polymers and pseudo synthetic polymers (such as

synthetic polypeptides), all of which are broadly used for hydrophobic drug delivery (Brocchini and Duncan, 1999). During the past decade, natural polymers including chitosan-based polymeric micelles have been studied for their potential as drug delivery vehicles (Qu et al., 2009; Yuan et al., 2010; Yu et al., 2012; Sahu et al., 2011b). Nevertheless, these reports used high molecular weight chitosan, in range that was >30 kDa. Certainly, the molecular weight is important characteristic to consider in a delivery system carrier. In the present study, low molecular weight chitosan (<15 kDa) was used as a component of a hydrophobic drug delivery system. The low molecular weight chitosan can be more easily and quickly degraded in the body compared to high-molecular-weight chitosan. In addition, PEG was conjugated to OCFP in order to provide the carrier with desirable attributes associated with PEGylation (such as the reduction or prevention of protein adsorption to increase a drug's half-life within the body, prolonging the activity of the drug, reducing the dosing frequency, and prolonging the lifetime of the carrier in plasma) (Allen et al., 2002; Elbert and Hubbell, 1996; Williams, 2008).

Cancer, a malignant neoplasm involving various diseases, is globally the leading cause of death, with the number of patients diagnosed with cancer increasing in developed countries. Paclitaxel (PTX) is an anticancer drug that is a clinically effective treatment for

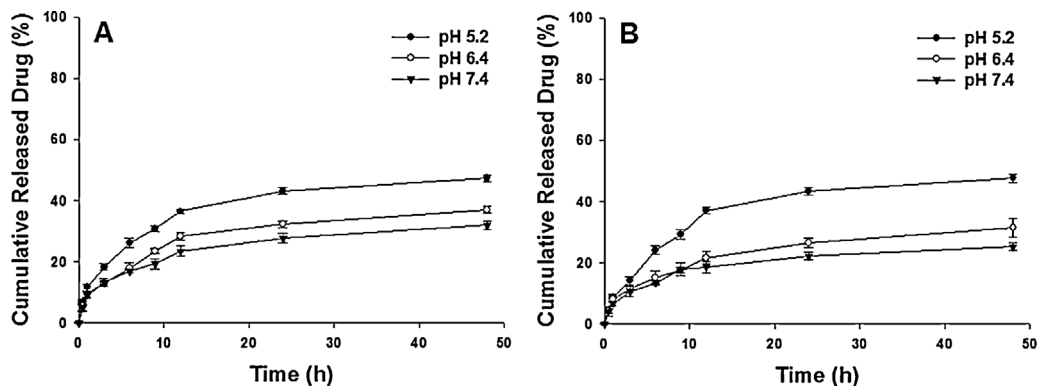


**Fig. 7.** Cumulative release profile of PTX from TPOCFP 5 (A) and TPOCFP 10 (B) micelles in phosphate buffer (pH 5.2, 6.4, and 7.4) at each time point (0.5–48 h) by using HPLC.

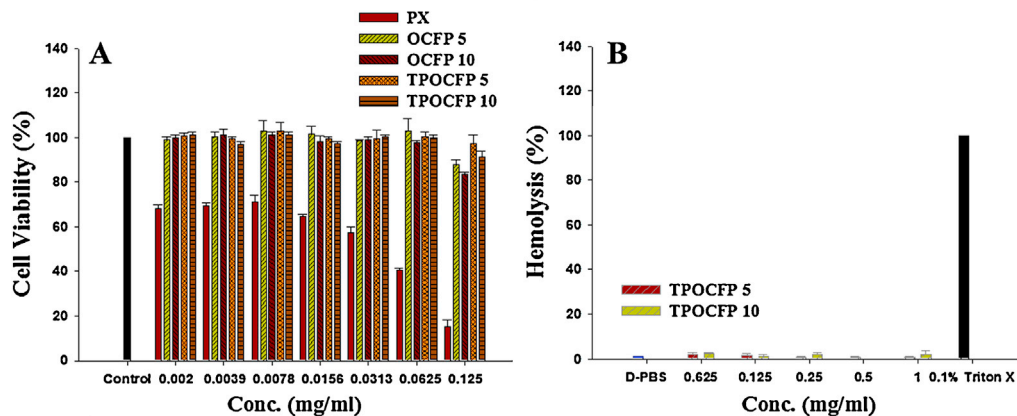


**Fig. 8.** In vitro cell cytotoxicity of the OCFP 5, OCFP 10, TPOCFP 5, and TPOCFP 10 in HEK 293 cell by MTT assay after incubation for 24 h (A) and hemolytic activity of TPOCFP 5 and TPOCFP 10 in RBC (B).

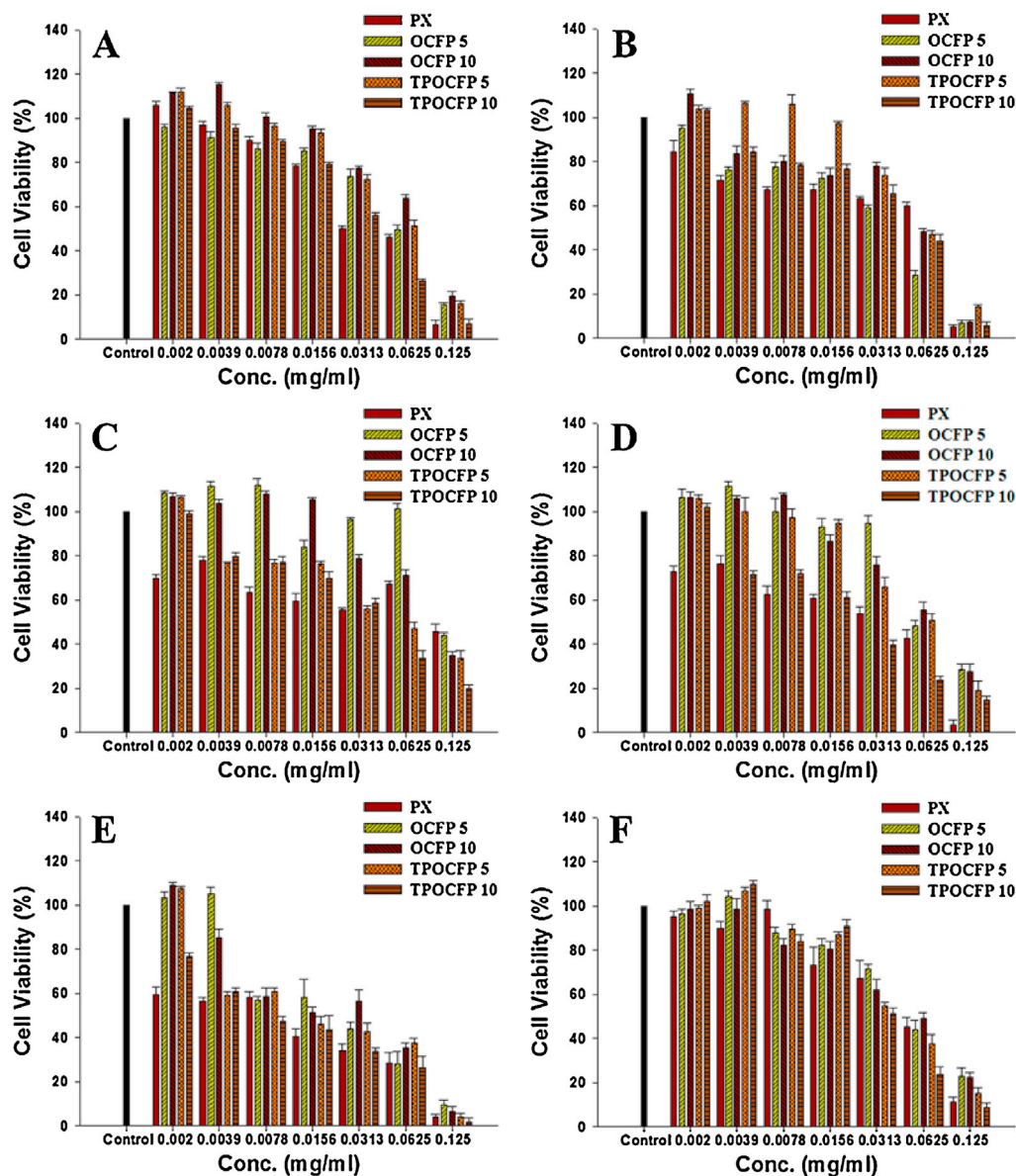


**Fig. 9.** Anticancer activity of PTX, OCFP 5, OCFP 10, TPOCFP 5, and TPOCFP 10 in various cancer cell lines such as LoVo cell (A), DLD-1 cell (B), CoLo 255 cell, (C) HCT 119 cell (D), PC3 cell (E), and SK-Br3 cell (F) by using MTT assay after incubated for 24 h.

various solid tumors, including non-small cell lung cancer, breast cancer, and ovarian cancer (Kim et al., 2001; Singla et al., 2002). However, the use of PTX has been limited due to serious side effects caused by Cremophor EL, which include allergic reactions, neurotoxicity, and nephrotoxicity in patients (Yao et al., 2011). Therefore, in this study, PTX was encapsulated in OCF micelles via hydrophobic interactions between the hydrophobic ligand (FA) of OCF and PTX, negating the need for Cremophor EL, and decreasing the cytotoxicity of PTX.

An increase in the variety of diseases affecting humans has resulted in the emergence of increasingly novel therapeutic drug carriers specifically designed as a treatment for a particular disease. An attractive strategy aimed at enhancing the cellular uptake of drug carriers is to engineer these drug carriers to possess site-specific recognition molecules. Transferrin can achieve site-specific targeting due to the high concentration of their receptors present on malignant cells (Richardson and Ponka, 1997; Huebers and Finch, 1987). During the past decade, many researchers studied transferrin conjugates in site-specific drug delivery system (Dufes

et al., 2004; Vaidya and Vyas, 2012; Anabousi et al., 2006). The results from these studies show high cellular uptake of polymeric vesicles by receptor-mediated endocytosis, mediated by transferrin and the TfR. However, within these systems, the ligand is covalently coupled onto preformed carriers, which has several disadvantages. Unreacted end groups can remain, and unwanted interactions with water molecules or with the drug itself can occur (Tomasina et al., 2013). In this present study, a target ligand-PEG-chitosan based carrier was synthesized to overcome this problem. This system, where ligand is conjugated through via the flexible PEG, assigns great flexibility and targeting efficiency of drug carrier.

The endocytic pathway, which mediates uptake of drug delivery systems by the cell, is very important for understanding the process of cellular uptake mechanisms, intracellular stability, and bioavailability of therapeutic agents. Therefore, many researchers have studied the endocytic pathway of various delivery carriers (Yuan et al., 2010; Ruiz et al., 2011; Fu et al., 2013). Five major cellular uptake mechanisms are distinguished, as follows: (1) phagocytosis, (2) clathrin-dependent endocytosis, (3) caveolin-mediated

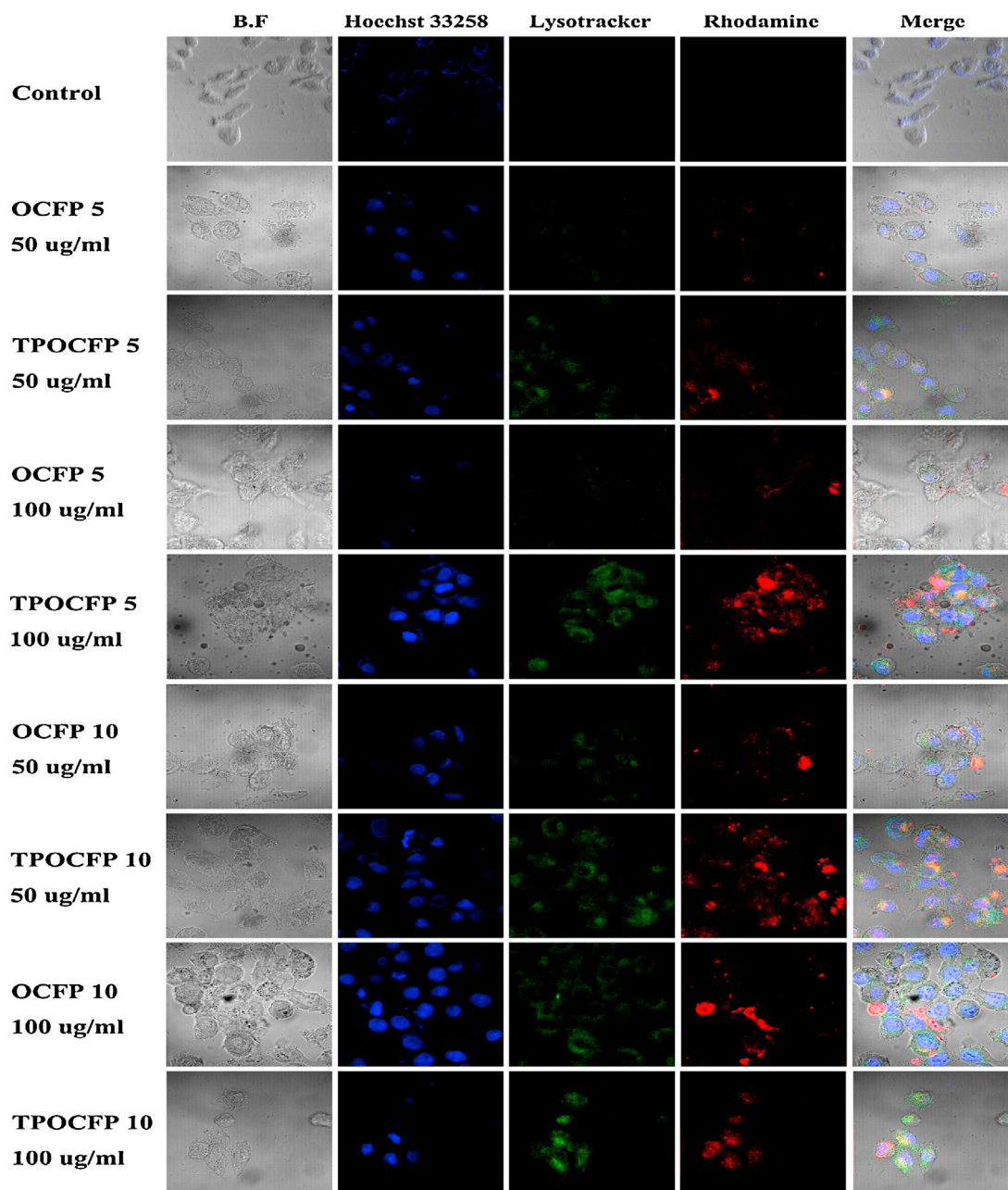


**Fig. 10.** Confocal laser scanning microscopy imaging of PC3 cells incubated with OCFP and TPOCFP micelles after incubated for 4 h. Micelles, lysosomes, and nuclei of cells were stained with rhodamine, LysoTracker and DAPI, respectively.

endocytosis, (4) macropinocytosis, and (5) clathrin- and caveolin-independent pathways (Khalil et al., 2006). Endocytosis can be strongly inhibited with metabolic inhibitors such as indomethacin, chlorpromazine, sodium azide, and colchicine. The agents used to inhibit specific endocytic pathways are as follows: indomethacin (10  $\mu$ M, caveolin-mediated endocytosis); chlorpromazine (10  $\mu$ M, clathrin-mediated endocytosis) (Chang et al., 2009); sodium azide (100 mM) and colchicine (15 mM, energy dependent processes) (Ruiz et al., 2011). Our FACS results showed that the TPOCFP micelles were taken up into the cell via clathrin-mediated endocytosis. This indicated that the transferrin associated with the TPOCFP micelle effectively bound to TfR present on the surface of cancer cells. In addition, CLSM provided evidence supporting clathrin-mediated endocytosis as the pathway through which these micelles are taken up by the cell.

In conclusion, we designed a novel drug carrier that is characterized by low cytotoxicity, high cellular uptake, sustained release, and site-specific targeting. The TPOCFP micelles satisfied all of these conditions. The TPOCFP micelles have a spherical shape, with a particle size of 140–649 nm. Drug release from TPOCFP micelles was less than 50% over 48 h. The TPOCFP micelle is non-toxic and has significant anticancer activity, as indicated by the MTT assay using a variety of cancer cell lines. In addition, the TF component of TPOCFP effectively targeted the TfR present on the surface of the cancer cell, and which efficiently mediated uptake into the cell through clathrin-mediated endocytosis. These mechanisms were clearly demonstrated in CLSM and FACS analysis. The results of this research indicate that the TP-conjugated TPOCFP micelles can serve as an effective treatment for solid tumors by targeting delivery and reducing toxicity and side effects of hydrophobic drugs. Additional

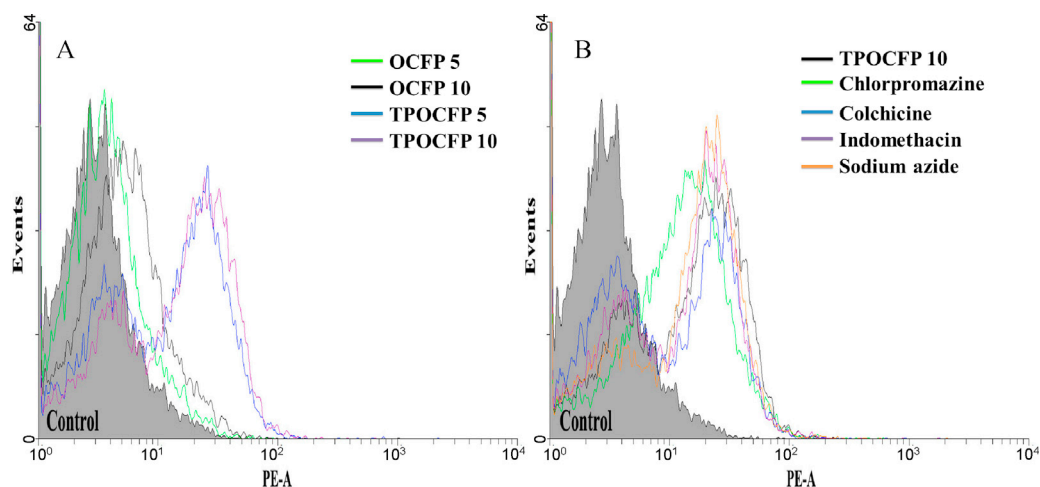


**Fig. 11.** Receptor mediated dependent cellular uptake of rhodamine-labeled OCFP and TPOCFP micelles and measured by flow cytometry. Flow cytometric logarithmic histogram of cells incubated with OCFP and TPOCFP micelles (A) and various inhibitor such as indomethacin (10  $\mu$ M), chlorpromazine (10  $\mu$ M), sodium azide (100  $\mu$ M), and colchicine (15  $\mu$ M) incubated before treated OCFP or TPOCFP micelles into the cells (B).

studies are in progress to determine the in vivo efficacy of TPOCFP micelles as a clinical therapy.

### Acknowledgements

This research was supported by Basic Science Research Program through the National Research Foundation of Korea (NRF) funded the Ministry of Education, Science and Technology (2011-0012039).

### References

- Allen, C., Dos Santos, N., Gallagher, R., Chiu, G.N., Shu, Y., Li, W.M., Johnstone, S.A., Janoff, A.S., Mayer, L.D., Webb, M.S., Bally, M.B., 2002. Controlling the physical behavior and biological performance of liposome formulations through use of surface grafted poly(ethylene glycol). *Biosci. Rep.* 22, 225–250.
- Anabousi, S., Bakowsky, U., Schneider, M., Huwer, H., Lehr, C.M., Ehrhardt, C., 2006. In vitro assessment of transferrin-conjugated liposomes as drug delivery systems for inhalation therapy of lung cancer. *Eur. J. Pharm. Sci.* 29, 367–374.
- Brocchini, S., Duncan, R., 1999. *Encyclopedia of Controlled Drug Delivery*. Wiley, New York, pp. 786–816.
- Burt, H.M., Zhang, X., Toleikis, P., Embree, L., Hunter, W.L., 1999. Development of copolymers of poly(D,L-lactide) and methoxypolyethylene glycol as micellar carriers of paclitaxel. *Colloids Surf. B: Biointerfaces* 16, 161–171.
- Chang, J., Jallouli, Y., Kroubi, M., Yuan, X.B., Feng, W., Kang, C.S., Pu, P.Y., Betbeder, D., 2009. Characterization of endocytosis of transferrin-coated PLGA nanoparticles by the blood–brain barrier. *Int. J. Pharm.* 379, 285–292.
- Chen, L.Y., Du, Y.M., Tian, Z.G., Sun, L.P., 2005. Effect of the degree of deacetylation and the substitution of carboxymethyl chitosan on its aggregation behavior. *J. Polym. Sci. Part B: Polym. Phys.* 43, 296–305.
- Chen, X.G., Park, H.J., 2003. Chemical characteristics of O-carboxymethyl chitosans related to the preparation conditions. *Carbohydr. Polym.* 53, 355–359.
- Cho, K., Wang, X., Nie, S., Chen, Z.G., Shin, D.M., 2008. Therapeutic nanoparticles for drug delivery in cancer. *Clin. Cancer Res.* 14, 1310–1316.
- Dufes, C., Muller, J.M., Couet, W., Olivier, J.C., Uchegbu, I.F., Schatzlein, A.G., 2004. Anticancer drug delivery with transferrin targeted polymeric chitosan vesicles. *Pharm. Res.* 21, 101–107.
- Elbert, D.L., Hubbell, J.A., 1996. Surface treatments of polymers for biocompatibility. *Ann. Rev. Mater. Sci.* 26, 365–394.
- Fu, Q., Sun, J., Ai, X., Zhang, P., Li, M., Wang, Y., Liu, X., Sun, Y., Sui, X., Sun, L., Han, X., Zhu, M., Zhang, Y., Wang, S., He, Z., 2013. Nimodipine nanocrystals for oral bioavailability improvement: role of mesenteric lymph transport in the oral absorption. *Int. J. Pharm.* 448, 290–297.
- Hong, M., Zhu, S., Jiang, Y., Tang, G., Sun, C., Fang, C., Shi, B., Pei, Y., 2010. Novel anti-tumor strategy: Peg-hydroxycamptothecin conjugate loaded transferrin-PEG-nanoparticles. *J. Control. Release* 14, 22–29.
- Huebers, H.A., Finch, C.A., 1987. The physiology of transferrin and transferrin receptors. *Physiol. Rev.* 67, 520–582.
- Huennekens, F.M., 1994. Tumor targeting: activation of prodrugs by enzyme-monoclonal antibody conjugates. *Trends Biotechnol.* 12, 234–239.
- Kainthan, R.K., Gnanamani, M., Ganguli, M., Ghosh, T., Brooks, D.E., Maiti, S., Kizhakkedathu, J.N., 2006. Blood compatibility of novel water soluble hyperbranched polyglycerol-based multivalent cationic polymers and their interaction with DNA. *Biomaterials* 27, 5377–5390.
- Khalil, I.A., Kogure, K., Akita, H., Harashima, H., 2006. Uptake pathways and subsequent intracellular trafficking in nonviral gene delivery. *Pharmacol. Rev.* 58, 32–45.
- Kim, S.C., Kim, D.W., Shim, Y.H., Bang, J.S., Oh, J.S., Wan, K.S., Seo, M.H., 2001. In vivo evaluation of polymeric micellar paclitaxel formulation: toxicity and efficacy. *J. Control. Release* 72, 191–202.
- Li, H., Qian, Z.M., 2002. Transferrin/transferrin receptor-mediated drug delivery. *Med. Res. Rev.* 22, 225–250.
- Liang, N., Sun, S., Li, X., Piao, H., Piao, H., Cui, F., Fang, L., 2012. a-Tocopherol succinate-modified chitosan as a micellar delivery system for paclitaxel: preparation, characterization and in vitro/in vivo evaluations. *Int. J. Pharm.* 423, 480–488.
- Liu, X.F., Guan, Y.L., Yang, D.Z., Li, Z., Yao, K.D., 2001. Antibacterial action of chitosan and carboxymethylated chitosan. *J. Appl. Polym. Sci.* 79, 1324–1335.
- Liu, Z., Jiao, Y., Wang, Y., Zhou, C., Zhang, Z., 2008. Polysaccharides-based nanoparticles as drug delivery systems. *Adv. Drug Deliv. Rev.* 60, 1650–1662.
- Nah, J.W., Jang, M.K., 2002. Spectroscopic characterization and preparation of low molecular water soluble chitosan with free-amine group by novel method. *J. Polym. Sci. Part A: Polym. Chem.* 40, 3796–3803.
- Nam, J.P., Kim, D.G., Kim, Y.B., Jeong, Y.I., Jang, M.K., Nah, J.W., 2008. Preparation and NMR spectroscopic characterization of low molecular water soluble O-carboxymethyl chitosan. *J. Chitin Chitosan* 13, 105–109.
- Perales, J.C., Ferkol, T., Molas, M., Hanson, R.W., 1994. An evaluation of receptor-mediated gene transfer using synthetic DNA–ligand complexes. *Eur. J. Biochem.* 226, 255–266.
- Qian, Z.M., Li, H., Sun, H., Ho, K., 2002. Targeted drug delivery via the transferrin receptor-mediated endocytosis pathway. *Pharmacol. Rev.* 54, 561–587.
- Qu, G., Yao, Z., Zhang, C., Wu, X., Ping, Q., 2009. PEG conjugated N-octyl-O-sulfate chitosan micelles for delivery of paclitaxel: in vitro characterization and in vivo evaluation. *Eur. J. Pharm. Sci.* 37, 98–105.
- Richardson, D.R., Ponka, P., 1997. The molecular mechanisms of the metabolism and transport of iron in normal and neoplastic cells. *Biochim. Biophys. Acta* 1333, 1–40.
- Ruiz, L.C., Fuente, M.D.L., Parraga, J.E., Garcia, A.L., Fernandez, I., Seijo, B., Sanchez, A., Calonge, M., Diebold, Y., 2011. Intracellular trafficking of hyaluronic acid-chitosan oligomer based nanoparticles in cultured human ocular surface cells. *Mol. Vis.* 17, 279–290.
- Sahu, S.K., Maiti, S., Maiti, T.K., Ghosh, S.K., Pramanik, P., 2011a. Folate decorated succinyl chitosan nanoparticles conjugated with doxorubicin for targeted drug delivery. *Macromol. Biosci.* 11, 285–295.
- Sahu, S.K., Mallick, S., Santra, S., Maiti, T.K., Ghosh, S.K., Pramanik, P., 2010. In vitro evaluation of folic acid modified carboxymethyl chitosan nanoparticles loaded with doxorubicin for targeted delivery. *J. Mater. Sci.: Mater. Med.* 21, 1578–1588.
- Sahu, S.K., Maiti, S., Maiti, T.K., Ghosh, S.K., Pramanik, P., 2011b. Hydrophobically modified carboxymethyl chitosan nanoparticles targeted delivery of paclitaxel. *J. Drug Target.* 19, 104–113.
- Sahu, S.K., Maiti, S., Pramanik, A., Ghosh, S.K., Pramanik, P., 2012. Controlling the thickness of polymeric shell on magnetic nanoparticles loaded with doxorubicin for targeted delivery and MRI contrast agent. *Carbohydr. Polym.* 87, 2593–2604.
- Senior, J.H., 1987. Fate and behavior of liposomes in vivo: a review of controlling factors. *Crit. Rev. Ther. Drug Carrier Syst.* 3, 123–193.
- Singla, A.K., Garg, A., Aggarwal, D., 2002. Paclitaxel and its formulations. *Int. J. Pharm.* 235, 179–192.
- Tomasina, J., Lheureux, S., Gauduchon, P., Rault, S., Freon, A.M., 2013. Nanocarriers for the targeted treatment of ovarian cancers. *Biomaterials* 34, 1073–1101.
- Vaidya, B., Vyas, S.P., 2012. Transferrin coupled vesicular system for intracellular drug delivery for the treatment of cancer: development and characterization. *J. Drug Target.* 20, 372–380.

- Vincent Lee, V.H., Hashida, M., Mizushima, Y., 1995. Trends and Trends and Future Perspectives in Peptide and Protein Drug Delivery. Harwood Academic Publications, Chur, Switzerland.
- Wang, N.X., Recum, H.A., 2011. Affinity-based drug delivery. *Macromol. Biosci.* 11, 321–332.
- Wang, Y., Liu, L., Weng, J., Qiqing, Z., 2007. Preparation and characterization of self-aggregated nanoparticles of cholesterol-modified O-carboxymethyl chitosan. *Carbohydr. Polym.* 69, 597–606.
- Williams, D.F., 2008. On the mechanisms of biocompatibility. *Biomaterials* 29, 2941–2953.
- Yang, J., Liu, Y., Wang, H., Liu, L., Wang, W., Wang, C., Wang, Q., Liu, W., 2012. The biocompatibility of fatty acid modified dextran-*agmatine* bioconjugate gene delivery vector. *Biomaterials* 33, 604–613.
- Yao, H.J., Ju, R.J., Wang, X.X., Zhang, Y., Li, R.J., Yu, Y., Zhang, L., Lu, W.L., 2011. The anti-tumor efficacy of functional paclitaxel nanomicelles in treating resistant breast cancers by oral delivery. *Biomaterials* 32, 3285–3302.
- Yin, C.H., Hou, C.L., Jiang, L.X., Gu, Q.S., 2004. Research on carboxymethyl chitosan acting as the adjuvant for implantable degradable microspheres. *J. Biomed. Eng.* 21, 350–354.
- Yokoyama, M., 1992. Block copolymers as drug carriers. *Crit. Rev. Ther. Drug Carrier Syst.* 9, 213–248.
- Yu, J., Xie, X., Wu, J., Liu, Y., Liu, P., Xu, X., Yu, H., Lu, L., Che, X., 2012. Folic acid conjugated glycol chitosan micelles for targeted delivery of doxorubicin: preparation and preliminary evaluation in vitro. *J. Biomater. Sci. Polym. Ed.* 24, 606–620.
- Yuan, H., Lu, L.J., Du, Y.Z., Hu, F.Q., 2010. Stearic acid-g-chitosan polymeric micelle for oral drug delivery: in vitro transport and in vivo absorption. *Mol. Pharm.* 8, 225–238.